Soft Matter

Micromechanical Characterization of Soft, Biopolymeric Hydrogels: Stiffness, Resilience, and Failure

Journal:	*Soft Matter*
Manuscript ID	SM-ART-03-2018-000501.R1
Article Type:	Paper
Date Submitted by the Author:	16-Apr-2018
Complete List of Authors:	Rattan, Shruti; University of Massachusetts Amherst, Department of Polymer Science and Engineering Li, Linqing; University of Delaware, Materials Science and Engineering Lau, Hang; University of Delaware, Materials Science and Engineering Crosby, Alfred; University of Massachusetts, Polymer Science and Engineering Kiick, Kristi; University of Delaware, Materials Science and Engineering

Soft Matter

Paper

Micromechanical Characterization of Soft, Biopolymeric Hydrogels: Stiffness, Resilience, and Failure

Received 00th January 20xx,
Accepted 00th January 20xx

DOI: 10.1039/x0xx00000x

www.rsc.org/

Shruti Rattan[a,+], Linqing Li[b,+], Hang Kuen Lau[b,+], Alfred J. Crosby[a,*] and Kristi L. Kiick[b,c,d,*]

Detailed understanding of the local structure-property relationships in soft biopolymeric hydrogels can be instrumental for applications in regenerative tissue engineering. Resilin-like polypeptide (RLP) hydrogels have been previously demonstrated as useful biomaterials with a unique combination of low elastic moduli, excellent resilience, and cell-adhesive properties. However, comprehensive mechanical characterization of RLP hydrogels under both low-strain and high-strain conditions has not yet been conducted, despite the unique information such measurements can provide about the local structure and macromolecular behavior underpinning mechanical properties. In this study, mechanical properties (elastic modulus, resilience, and fracture initiation toughness) of equilibrium swollen resilin-based hydrogels were characterized via oscillatory shear rheology, small-strain microindentation, and large-strain puncture tests as a function of polypeptide concentration. These methods allowed characterization, for the first time, of the resilience and failure in hydrogels with low polypeptide concentrations (< 20wt%), as the employed methods obviate the handling difficulties inherent in the characterization of such soft materials via standard mechanical techniques, allowing characterization without any special sample preparation and requiring minimal volumes (as low as 50 μL). Elastic moduli measured from small-strain microindentation showed good correlation with elastic storage moduli obtained from oscillatory shear rheology at a comparable applied strain rate, and evaluation of multiple loading-unloading cycles revealed decreased resilience values at lower hydrogel concentrations. In addition, large-strain indentation-to-failure (or puncture) tests were performed to measure large-strain mechanical response and fracture toughness on length scales similar to biological cells (~10–50 μm) at various polypeptide concentrations, indicating very high fracture initiation toughness for high-concentration hydrogels. Our results establish the utility of employing microscale mechanical methods for the characterization of the local mechanical properties of biopolymeric hydrogels of low concentrations (< 20 wt%), and show how the combination of small and large-strain measurements can provide unique insight into structure-property relationships for biopolymeric elastomers. Overall, this study provides new insight into the effects on local mechanical properties of polypeptide concentration near the overlap polymer concentration c* for resilin-based hydrogels, confirming their unique elastomeric features for applications in regenerative medicine.

Introduction

Resilin is a well-known elastomeric, structural protein normally present in the specialized regions of most insects' cuticle compartments to provide efficient energy storage and release in order to support mechanical function during jumping, flight, and sound production.[1–4] Naturally crosslinked resilin exhibits unique rubber-like features, including high resilience, reversible extensibility at large strains, and high-efficiency energy transfer. Although mechanically similar to other elastomeric proteins, compositionally, resilin is substantially more hydrophilic than natural elastins, collagens or silks.[5–8] Owing to widespread interest in the outstanding mechanical properties of natural resilin, tremendous efforts have been devoted to fabricating synthetic resilin-based materials as a new class of bio-elastomers for mechanically demanding applications, including in regenerative medicine (e.g., in treating vocal fold pathologies).[9–13] Facilitated by the routine application of recombinant DNA technology, multiple resilin-like polypeptides (RLPs), based on the consensus sequences decoded from the *Drosophila melanogaster* and *Anopheles gambiae* resilin genes, have been produced.[14–16] The biopolymers have been used to generate a library of biomaterials, in the forms of hydrogels, films, nanoparticles,[17,18] fibers[19,20] and biocomposites,[21–23] with tunable protein structure, physicochemical behavior, and superior mechanical properties. RLPs have also been designed to include other peptide/protein domains to permit simulation of the passive elasticity of muscle protein,[10] to induce assembly,[20] as well as to capture the biophysical and biochemical characteristics of native ECM microenvironments[24] to accelerate and promote cell differentiation for vocal fold,[13,25] bone[26] or vascular tissue

[a] Polymer Science and Engineering Department, University of Massachusetts Amherst, 120 Governors Drive, Amherst, Massachusetts, 01003, USA.
[b] Department of Materials Science and Engineering, University of Delaware, 201 DuPont Hall, Newark, Delaware, 19716, USA.
[c] Department of Biomedical Engineering, University of Delaware, Newark, Delaware, 19716, USA.
[d] Delaware Biotechnology Institute, 15 Innovation Way, Newark, Delaware, 19711, USA.
† These authors contributed equally to this work.
Electronic Supplementary Information (ESI) available: [details of any supplementary information available should be included here]. See DOI: 10.1039/x0xx00000x

engineering.[27] The RLP-based materials show high cell viability for human mesenchymal stem cells[13,25] and aortic adventitial fibroblasts in 3D cell culture,[11,21] as well as high biocompatibility after subcutaneous implantation and direct injection *in vivo* (subcutaneous and in vocal fold tissue),[13] demonstrating the potential of appropriately engineered RLPs for tissue engineering applications.[13,25,28,29]

We have designed and synthesized multiple versions of RLPs comprising 12 repeats of the consensus motif $(GGRPSDS(F/M)GAPGGGN)_n$ and 5 repeats of a lysine-rich crosslinking bundle (GGKGGKGGKGG) that can be crosslinked *via* various chemistries, including phosphine-mediated crosslinking,[4,13] Michael-type additions, UV-initiated radical polymerization, and thiol-ene reactions to form elastomeric hydrogels that exhibit reversible elasticity, minimum stress relaxation and large strain-to-break values with high resilience.[29,30] To date, the superior mechanical properties of synthetic RLP-based materials (elastic moduli ~ 5000 Pa, polypeptide concentration ~20 wt%) have been characterized and validated generally *via* oscillatory shear rheology, uniaxial tensile testing, torsional-wave apparatus high frequency rheology, and scanning probe microscope techniques focused primarily on measuring macroscale materials mechanics.[9,29,30] However, systematic mechanical measurement studies over a range of polypeptide concentrations to investigate the evolution of structure that may contribute to the exceptional mechanical properties of RLP materials have not yet been conducted, in large part owing to practical issues in the handling of soft hydrogels (elastic moduli in the range of 500-1000 Pa) during traditional mechanical measurement techniques. Moreover, there has thus been a dearth of information about the mechanical response of these materials across a wide range of applied deformations and very limited characterization of failure at micron length scales. We thus sought to apply new methods for the characterization of these highly soft materials to understand the influence of underlying structure on macroscopic mechanical response at various polypeptide concentrations.

Hydrogel crosslinking methods can be generally categorized by *in situ* chemical crosslinking of monomers (or functionalized macromolecules) or physical interconnection of macromolecules. Macromolecular crosslinking via end-group or side-chain coupling provides better control over the polymer network architecture compared to uncontrolled radical polymerization of monomers and crosslinkers.[31,32] Hydrogel inhomogeneities exhibited in crosslinked polymer networks or defects, such as dangling chain ends, loops, free chains, and multiple crosslinking sites, often impact physical properties of the hydrogels including elasticity, swelling, and permeability.[33–35] Several attempts have been made to quantitatively predict elastic moduli by excluding elastically ineffective chains or defects in polymer networks.[36–39] However, those models have been applied for different classes of synthetic polymer networks with controlled crosslinking chemistries and have not been well developed for biopolymeric materials. For random-coil polymer solutions, there are three concentration regimes corresponding to

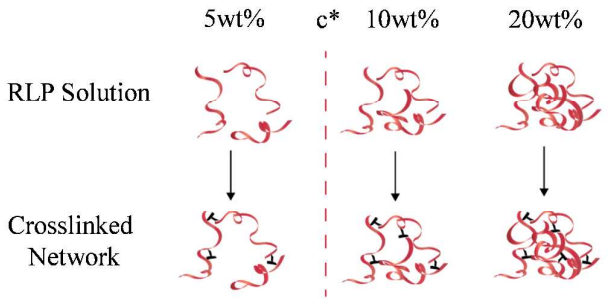

Figure 1 Schematic of RLP chains in solution and in crosslinked networks at concentrations near the overlap polypeptide concentration, c* (ranging from 5-20wt%).

separated chains (dilute), overlapping chains (semi-dilute), and congested chains (concentrated); the overlap concentration (c*) is defined as the crossover polymer concentration from dilute to the semi-dilute solution regime.[40] Polymer solution concentrations above the overlap concentration are required for effective inter-chain crosslinking, which occurs only at inter-chain contact points,[35] while polymer solutions below the overlap concentration will form sparse networks in which reacted polymer chains cannot fill the entire volume.[41] In this work, we adopted resilin-based hydrogels to understand the formation of networks and the corresponding micromechanical properties in RLP hydrogels as a function of polypeptide concentrations around the overlap polypeptide concentration, c* (**Figure 1**).

In order to study the influence of network evolution with increasing concentration on mechanical response, we employed oscillatory shear rheology, small-strain microindentation, along with a novel, custom-built mechanical method to characterize large-strain indentation and fracture initiation at length scales ranging from sub-millimeter to a millimeter **(Figure 2)**. Oscillatory shear rheology and small-strain microindentation measure the small-strain elastic response of RLP hydrogels, microindentation, in particular, providing information on the local mechanical response of the material subjected to small deformations or strains at any arbitrary location on the surface.[42] To complement small-strain measurements, large-strain indentation and puncture provide insight regarding the material's mechanical response at large deformations as well as the resistance for fracture initiation.[43] In addition to providing important mechanical property measurements, microindentation and puncture studies require minimum sample preparation and volume, offer ease of implementation, and can be used for *in vivo* characterization of soft material implants as well as biological tissues and organs. Previous applications of such techniques on various other synthetic polymer gels and biological tissues have validated the robustness of these methods in quantifying the mechanical properties and correlating them with measurements from bulk mechanical testing techniques, such as oscillatory shear rheology, and uniaxial tensile tests.[43–45] Overall, we correlate the mechanical response of RLP materials to their network structure and polymer chain interactions at various polypeptide concentrations, and highlight the ability to

tailor mechanical response. With a better understanding of the structural evolution in RLP hydrogels around the overlap polypeptide concentration, more sophisticated design of RLP materials as soft tissue scaffolds for regenerative medicine should be possible.

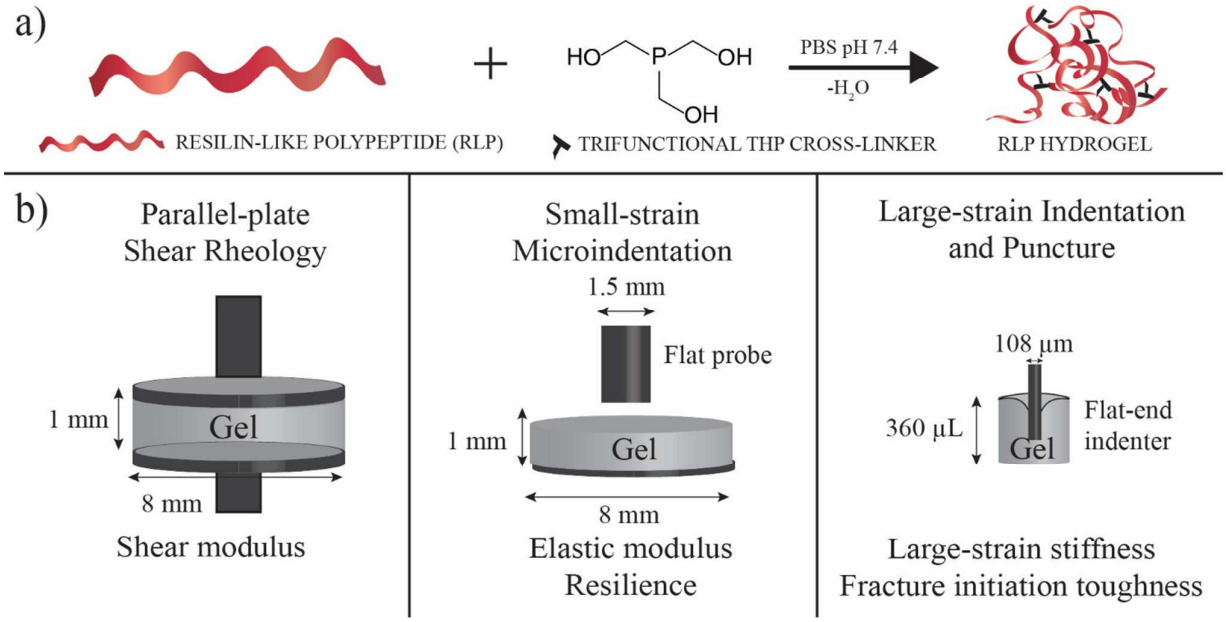

Amino acid sequence of RLP:
MRGSHHHHHHGSRS-GGKGGKGGKGG-(GGRPSDSXGAPGGGN)$_3$-LQ-*GGKGGKGGKGG*-LQ-(GGRPSDSXGAPGGGN)$_3$-VD-*GGKGGKGGKGG*-VD-(GGRPSDSXGAPGGGN)$_3$-EL-*GGKGGKGGKGG*-EL-(GGRPSDSXGAPGGGN)$_3$-*GGKGGKGGKGG*-GT
***GGKGGKGGKGG*: lysine-containing crosslinking domain**
GGRPSDSXGAPGGGN: resilin-derived putative consensus sequence, residue X=F or M

Figure 2 (a) Schematic of crosslinking reaction for resilin-based hydrogels. (b) Schematic of the three mechanical measurement techniques namely, oscillatory shear rheology, small-strain microindentation, and large-strain blunt puncture mechanics used to characterize RLP hydrogels. The full amino acid sequence of the resilin-like polypeptide employed is also provided for reference.

Materials and Methods

Formation of resilin-like polypeptide-based hydrogels

Resilin-like polypeptides were expressed and purified as previously described with a final product yield of approximately 20-30 mg/L after dialysis and lyophilization.[25] RLP hydrogels at different polypeptide concentrations were crosslinked using tri(hydroxymethyl) phosphine (THP)-based condensation reaction following previously established protocols.[25,28,29] RLP precursor solutions (~50 μL) were added in circular silicone molds with 8 mm diameter and 1 mm thickness for gelation at 37^{o}C for 2 hours for rheology and small-strain microindentation characterization. RLP precursor solutions (~360 μL) were added to 96-well plates with a concentration of THP added to yield a 1:1 (amine: hydroxymethyl phosphine) molar ratio; cylindrical hydrogels with a height ~10 mm and diameter ~6 mm were prepared for puncture mechanics. Hydrogels were incubated at 37^{o}C for 2 hours for complete gelation followed by hydration overnight in PBS before testing. Crosslinking efficiencies for all RLP hydrogel concentrations were quantified *via* amino acid analysis, with values summarized in **Table 1**. The amino acid analysis permits the calculation of the number of lysines reacted after hydrogel formation, and the crosslinking efficiency is defined as the calculated number of reacted lysines divided by the total number of lysine residues.

Oscillatory rheology

The oscillatory rheology experiments were conducted on an AR 2000 rheometer using 8 mm diameter stainless steel parallel-plate geometry. The swollen hydrogels were prepared as described above. The preformed hydrogels were mounted on the rheometer plates at room temperature (20ºC), and the geometry was set at a gap at which the normal force equalled 0.02 N to prevent slippage. Frequency sweep experiments, from 0.628-25 rad/s, were performed at a fixed strain amplitude of 1%, which is in the linear viscoelastic regime of the hydrogels as determined by a strain sweep at a fixed frequency of 1 Hz. Shear storage moduli (G') and loss moduli (G") were recorded over the entire frequency range with ten data points per decade. Experiments were repeated on three individual, separate samples for each polypeptide concentration.

Small-strain microindentation

RLP hydrogels at three different polypeptide concentrations (5wt%, 10wt% and 20wt%) were prepared on microscope glass slides. A piezo-controlled linear actuator was used to bring a cylindrical probe of radius, a = 750 μm, in contact at a constant

displacement rate of 10 μm/s with thin circular disks of hydrogels (thickness, h~1mm) rigidly adhered to glass coverslips. It is well known that soft polymer gels often have strain rate-dependent mechanical properties.[29,46–48] In order to facilitate comparison of low-strain elastic moduli between small-strain microindentation and rheology, a small indentation rate was chosen in order to yield quasi-static loading conditions during the experiments. The average strain rate for microindentation was computed from the indentation rate and the radius of the probe used, (average strain rate = (10 μm/sec)/(750 μm)) and was calculated as ~0.01Hz. Visualization of the contact area was enabled *via* use of a Zeiss Axiovert 200M microscope (Carl Zeiss, Oberkochen, Germany) and was used to confirm complete contact, where the established contact radius equalled the radius of the probe. Upon loading and unloading, the relative displacement, δ, and resulting force, P, was measured with a custom-designed load cell. Average stresses were calculated from the force normalized by the cross-sectional area of the probe

$$\left(\sigma = \frac{P}{\pi a^2}\right)$$

and average strains were calculated by normalizing the displacement by the radius of the probe ($\epsilon = \delta/a$) for 10wt% and 20wt% hydrogels (h~1000μm), and by the gel thickness ($\epsilon = \delta/h$) for 5wt% hydrogels (h~500μm).

Repeated loading and unloading cycles were performed for all compositions of RLPs to measure the reversible energy storage capability or resilience at different peak loads (or applied strains). Resilience is defined as the ability of a material to undergo significant deformations with minimum energy loss, and is measured by dividing the area under the unloading curves by the area under the loading curves.[10,49,50] Experiments were repeated at least 3 times on three different samples at each peak load. In order to quantify an effective linear elastic moduli, $E_{indentation}$ for the three hydrogel concentrations, a linear approximation was employed up to ~10% strain for the force-displacement curves obtained from the loading regime of the stress-strain cycles. Examples of the fit for three different loading curves for each hydrogel concentration are provided in **Figure S1** (a-c). The effective elastic modulus, $E_{indentation}$, was then determined from the slopes of the linear fits at low strain using the following equation:[51]

$$E_{indentation} = \frac{(1-\upsilon^2)}{2Ca}\left\{1 + 1.33\left(\frac{a}{h}\right) + 1.33\left(\frac{a}{h}\right)^3\right\}^{-1}$$

where the compliance, $C, (C = \partial\delta/\partial P)$, is the inverse of the slope of the linear force-displacement curve (during loading); υ is the Poisson's ratio (which was approximated as 0.5 assuming incompressibility under time scales of loading[52]); and h is thickness of the hydrogel sample. The average of the slopes obtained from the loading curves was used to quantify C. Note that equation (1) includes corrections for finite values of a/h, which deviate from the classical constraints of Hertzian contact mechanics.[42,51]

Large-strain indentation and puncture mechanics

For puncture experiments, the experimental set-up used for small-strain microindentation was utilized to perform large-strain indentation to the point of failure with hollow, flat-end needles with a tip inner radius, R, equal to 54 μm. Upon indentation, the force increases as the needle deforms the hydrogel until fracture occurs at a peak puncture force, P_c. Fakhouri *et al* have proposed semi-empirical relationships to analyze the force-displacement response during loading until the point of puncture in terms of the material's elastic modulus, E, and the needle tip geometry.[43] The deformation behavior of a material is modeled by Hertzian contact mechanics under small strains, and a Neo-Hookean model under large strains to develop the 'puncture equation':[43]

$$P = k''ER\delta + k'E\delta^2$$

where P is the resistive force on the indenter, δ is the indentation depth, R is the indenter tip radius, k' is an empirical constant, and k" is a constant depending upon indenter tip geometry, obtained from Hertzian contact mechanics for flat and spherically tipped indenters.[53]

Results

Estimation of crosslink density from amino-acid analysis

The crosslink density of the RLP hydrogels was determined by quantifying the difference in the amount of lysines that were reacted before and after crosslinking. The crosslinking efficiencies for 5wt%, 10wt%, and 20wt% RLPs were calculated as approximately 30% (**Table 1**); such consistency in the crosslinking efficiency across various polypeptide concentrations may be expected as the crosslinker ratio between lysine residues and functional hydroxymethylphosphine groups was maintained at 1:1 for all hydrogel concentrations. The number of crosslinks per unit volume, or the crosslinking density (ν_o), was estimated from the number of lysines reacted using the formula

$$\nu_o = \frac{c\,N_k}{f M_w}$$

where c is the concentration of RLP solution (g/L), N_k is the number of lysines reacted per RLP, f is the functionality of the cross-linker (f=3 for THP), and M_w is the molecular weight of RLP (g/mol). Accordingly, the crosslinking density, ν_o (mol/L) in each sample (summarized in Table 1) increases linearly with the increase of polypeptide concentration owing to the constant ratio of crosslinker to polypeptide.

Table 1 Crosslinking efficiency and crosslinking density of the RLP hydrogels quantified *via* amino acid analysis

Concentration (wt%)	Lysine Crosslinking efficiency (%)	Crosslinking density, ν_o (mol/L)
5	29.8±4.6	0.0032±0.0005
10	31.6±4.6	0.0068±0.0010
20	30.4±3.7	0.0131±0.0015

Small-strain elastic moduli: Oscillatory shear rheology and microindentation

Oscillatory shear rheology was employed to characterize the mechanical properties of preformed, equilibrium swollen RLP hydrogels under shear, and frequency sweep experiments were conducted to obtain shear storage moduli, G′ (averaged for n=3). Average shear storage moduli (G′) and loss moduli (G″) are plotted as a function of frequency over 0.628-25 rad/s and the data are shown in **Figure 3(a)**. RLP hydrogels at 10wt% and 20wt% exhibited frequency-independent deformation response suggesting their highly elastic nature, and the G′ values averaged over the frequency range, G'_{avg} were 478±51 Pa and 4374±130 Pa for 10wt% and 20wt% RLP hydrogels, respectively. 5wt% RLP hydrogels were not characterized by oscillatory shear rheology due to their extremely fragile nature, which led to challenges in sample preparation, handling, and loading of undamaged hydrogel onto the rheometer plate for measurement.

Small-strain microindentation was employed to perform repeated loading and unloading cycles at different applied peak loads to probe the deformation response under small strains and determine linear elastic modulus, and to calculate the resilience of hydrated RLP hydrogels. Representative stress-strain curves for RLP hydrogels at three concentrations, with a maximum applied average strain of ~20%, are shown in **Figure 3(b).** As illustrated in the data, the stress-strain curves for the three concentrations across all samples are relatively linear at small strains marked by the initial 'toe' region; however, at large deformations (see **Figure 4(a-c)**) the materials become stiffer and demonstrate a J-shaped curve typical of soft biological tissues[54] and fibrous synthetic biomaterials.[55] The slope of the initial linear regime of the stress-strain curves, which is a measure of elastic modulus, increases with increasing polypeptide concentration. The elastic moduli $E_{indentation}$, calculated from small-strain microindentation measurements using Equation 1, are 0.45 ± 0.06 kPa for 5wt%, 1.83 ± 0.61 kPa for 10wt%, and 11.65 ± 1.25 kPa for 20wt% hydrogels, respectively.

To provide comparisons to the properties measured through small-strain microindentation and oscillatory shear rheology, elastic storage moduli, $E_{rheology}$, were calculated from frequency-averaged shear storage moduli, G'_{avg} assuming hydrogel incompressibility, so that $E_{rheology}= 3G'_{avg}$. The elastic moduli calculated from shear rheology were 1.32 ± 0.06 kPa for 10wt%, and 12.18 ± 0.7 kPa for 20wt% hydrogels. Average values of $E_{indentation}$ and $E_{rheology}$ for all polypeptide concentrations are plotted against concentration in **Figure 3(c)** for comparison. The elastic modulus measurements from shear rheology are in good agreement with moduli measurements obtained from microindentation.

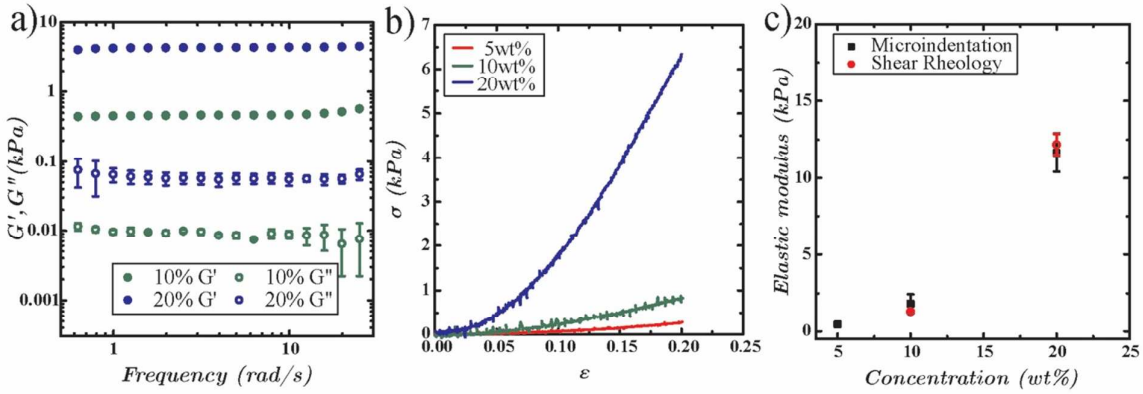

Figure 3 (a) Frequency sweep of oscillatory rheology with representative average shear moduli of preformed 10wt% (green) and 20wt% (blue) RLP hydrogels. The storage modulus G′ (solid) and loss modulus G″ (open) are both presented; (b) Stress-strain loading curves during small-strain microindentation for 5wt%, 10wt%, and 20wt% RLP hydrogels, presented up to a strain of ~20%. (c) Summary of the microscale elastic modulus measured from small-strain microindentation with elastic moduli obtained from oscillatory shear rheology at a comparable applied strain rate. Please note that the data in Figure 3(c) reflects error from calculations of elastic moduli from the stress-strain curves measured across different samples (n=3). Error bars from linear regression up to small strains of individual curves are smaller than error bars obtained from data averaged across different samples.

Small-strain microindentation: resilience

One of the major challenges of tissue engineering is to develop biomaterials that mimic the non-linear response of biological tissues under loading and unloading, while maintaining the ability to undergo deformation without appreciable loss in energy (high resilience); the resilience of RLP hydrogels thus was determined by comparing the areas under the loading and unloading curves in the small-strain microindentation experiments. Representative stress-strain cycles with different maximum applied loads for each RLP polypeptide concentration are shown in **Figure 4(a-c)**, with darker shades representing greater maximum applied loads. For 5wt% RLP hydrogels, repeated stress-strain cycles were performed at maximum applied loads of 0.5, 2.5, 5, and 9.5mN corresponding to resilience values 61.11±2.34%, 30.6±0.95%, 21.86±1.27%, and 26.08±1.28% respectively. For 10wt% RLPs, repeated stress-strain cycles were performed at maximum

applied loads of 5, 10, 13.5, and 20mN with resilience values 71.22±4.92%, 63.23±3.21%, 62.79±1.63%, and 55.34±2.38% respectively. Finally, for 20wt% RLPs, repeated stress-strain cycles were performed at maximum applied loads of 5,15, 30, 55, and 72mN to obtain corresponding resilience values as 82.64±1.22%, 84.52±0.29%, 78.99±2.35%, 76.7±1.44%, and 72.37± 0.81% respectively. Loading and unloading curves for 20wt% RLPs were superimposable up to ~25% strains and minimal hysteresis was observed, indicating high resilience (~85% for 20wt% RLPs) for these materials at low strains. For all concentrations, hysteresis increases with the increase of maximum strain applied as shown in **Figure 4(d),** indicating a decrease in resilience at higher strains.

The loss tangent,

$$\tan(\delta) = \frac{G''}{G'}$$

was also determined from oscillatory shear rheology data to provide a relative measure of the viscous to elastic properties of a material. Upon comparison of tan (δ) for the 10wt% and 20wt% hydrogels, we find that 10wt% hydrogels show a higher tan (δ) (~0.02) than that observed for the 20wt% hydrogels (~0.013); this difference is consistent with reported behaviour for a range of elastomers which exhibit lower energy storage with increasing loss tangent.[56–58]

Puncture mechanics

Puncture experiments offer advantages in the characterization of failure in soft gels, particularly in comparison to traditional tensile-to-rupture or notch tests, due to ease of implementation and minimum sample volume requirements. Moreover, traditional failure characterization techniques require the presence of an initial crack in the material and thus provide information about failure properties related to crack

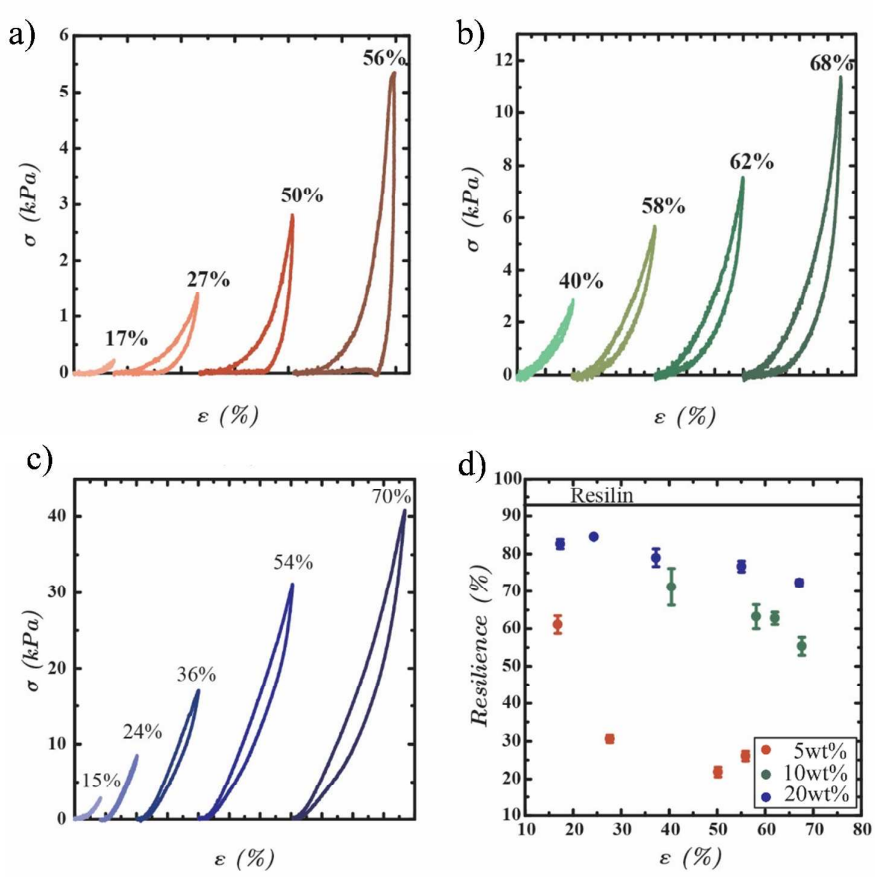

Figure 4 (a-c) Representative loading and unloading stress-strain cycle for 5wt%, 10wt% and 20wt% RLP hydrogels, respectively from microindentation experiments at different applied strains; stress-strain curves are offset with respect to one another for clarity. (d) Summary of averaged resilience values versus applied strains for three different RLP polypeptide concentrations.

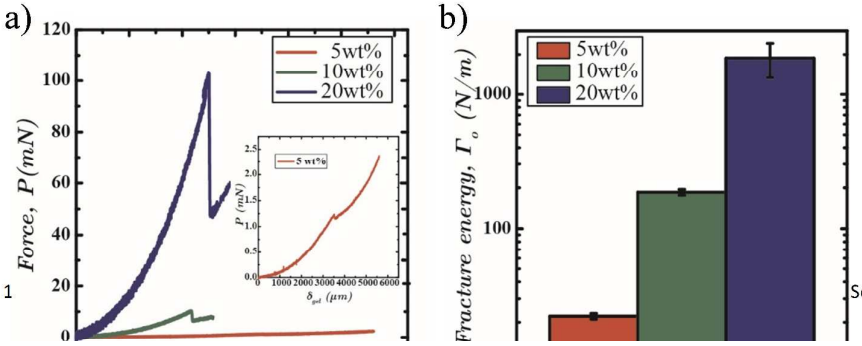

Figure 5 (a) Representative force-displacement curves for puncture experiments with a flat-end indenter of tip inner radius R=54μm for various concentrations of RLP hydrogels. The inset shows the force-displacement curve for a 5wt% hydrogel. (b). A bar plot comparing fracture initiation energy measured from puncture mechanics for the three RLP polypeptide concentrations. Note log scale on y-axis, demonstrating nonlinear increase in fracture resistance.

propagation rather than inherent resistance to fracture initiation. Large-strain indentation and puncture experiments were performed for RLP hydrogels using a flat-end indenter to provide insight into inherent material properties associated with fracture initiation, or the nucleation of a crack. The objective of conducting these measurements was to characterize the effective stiffness of RLP hydrogels at large strains to the point of failure, which is not captured by the low-strain linear elastic response obtained from microindentation tests. **Figure 5(a)** shows representative force-displacement curves for puncture experiments for the three concentrations of RLPs. Force-displacement curves for RLPs were fitted with Equation 2 to obtain effective elastic moduli value k'E for all compositions. Importantly, k'E is a measure of the large-strain response of materials and has been shown to correlate well with elastic moduli measurements from standard macroscale mechanical testing techniques, such as shear rheology, for various polymer gels and elastomer materials.[43] In addition to measuring k'E, puncture experiments provide a convenient, insightful measurement of the failure processes for soft, polymer gels. The critical puncture event at which the needle fractures the surface of the material is characterized by a sharp drop in force, as shown in the force-displacement curves for three RLP polypeptide concentrations in **Figure 5(a)**. The peak force at puncture, P_c, can be related to the critical nucleation stress or critical nucleation energy for fracture formation, depending on the size scale of the indenting probe radius.[43] The measured P_c value drastically increases with increasing RLP polypeptide concentration, exhibiting values from approximate 1mN for 5wt% RLP to 10mN and 100mN for 10wt% and 20wt% RLP hydrogels, respectively. Fracture initiation energies Γ_o, calculated by

$$\Gamma_o = \frac{P_c}{R}$$

also increase with the increase in RLP polypeptide concentrations, yielding on average value of 22J/m^2, 185J/m^2, 1875J/m^2 for 5wt%, 10wt% and 20wt% RLP hydrogels, respectively. A summary of the different metrics measured from the large-strain indentation and puncture experiments are listed in **Table 2**.

Table 2 Material properties associated with fracture initiation quantified using puncture mechanics

Concentration (wt%)	P_c (mN)	k'E (kPa)	Fracture initiation energy, Γ_o (J/m^2)
5	1.2±0.1	0.10±0.02	22.2±1.1
10	10.0±0.5	2.1±0.2	185±9.3
20	101±29	15.8±2.8	1870±540

Discussion

In this study, we adopt resilin-based hydrogels at various concentrations as a model material system and employ multiple mechanical characterization techniques to understand structure-property relationships via quantitative measurement of crosslink density, elastic moduli, resilience, and fracture initiation energy at different length scales. The measurement methods facilitate description of the measured properties of the RLP hydrogel networks with respect to potential structural heterogeneities, and these elastomeric hydrogels provide a unique system for expanding our current understanding of elastic response and failure in soft biopolymeric materials.

The results from the three different mechanical measurements of RLP hydrogels at various concentrations provide new understanding of how the mechanical properties in RLP materials correlate with the network structure at concentrations below, around, and above c*. Oscillatory shear rheological characterization of preformed, equilibrium swollen RLP hydrogels exhibited frequency independent behavior, which indicates the expected highly elastic nature of the covalently crosslinked RLP hydrogels. However, resilience measurements for various concentrations via small-strain microindentation show that loading and unloading curves become non-superimposable at high strains, suggesting that these RLP hydrogels have dissipative mechanisms that result in decreased resilience values at increased deformation. Specifically, 5wt% RLP hydrogels exhibited a drastic decrease in resilience with the increase of applied strain in comparison to 10wt% and 20wt% hydrogels (**Figure 4(a-c)**), and the corresponding resilience values at each strain are also significantly lower (**Figure 4(d)**). In fact, in addition to the observed cyclic hysteresis, the 5wt% hydrogels exhibit a permanent set (**Figure 4(a)**), indicating the flow of disconnected network components or the onset of fracture within the material due to incomplete network formation. The observation of a permanent set upon unloading during cyclic tensile and compression tests is attributed to the poor mechanical properties common in rubbers and hydrogels, and is generally attributed to viscoelastic flow and microstructural changes in the networks.[59,60]

To elucidate potential origins for this significant change in resilience with concentration in RLP hydrogels, we calculated the overlap concentration of the random-coil RLP[61,62]

$$c^* = \frac{M_w}{N_A(2R_g)^3}$$

where N_A is the Avogadro's number and R_g is radius of gyration of RLP. The R_g of RLPs is reported in previously published literature to be in the range of 3.5- 5.0 nm,[63] hence the corresponding range of c* is calculated as 50-140 g/L (or 5-14wt% RLP). The RLP used in our study has an R_g of approximately 3.8 nm (as assessed from preliminary SAXS data, not shown), which is close to literature values for other RLPs and which yields a c* of 8.75wt% (**Figure S2**). The remarkably low resilience measured for the 5wt% RLP networks is thus consistent with network formation at a concentration below c*, which upon crosslinking, would be expected to yield a loosely connected network with limited inter-chain crosslinking interactions, and increased network

defects, within the sample volume,[41] consistent with other biopolymer hydrogels crosslinked below c*.[64,65] As RLP polypeptide concentration is increased to 10wt% and 20wt%, the resulting networks are formed near or above c*, leading to more effective inter-chain crosslinking reactions with decreased network defects; thereby resulting in not only significant improvements in resilience values but also a lack of permanent deformation upon unloading (**Figure 4(b) and 4(c)**). The enhanced resilience at higher RLP concentrations is consistent with an increase in intrinsic intermolecular association, which in these networks likely involve both RLP chains and water molecules (e.g., dipolar interactions and hydrogen bonding), given the high percentage of polar residues in the RLP amino acid sequence. These dynamic non-covalent interactions contribute to a more homogeneous network formation with reduced defects.[66] Although the classical c* theorem by De Gennes predicts prepolymer concentrations above c* essential at preparation conditions for formation of a gel[67], gel formation at concentration below c* have been reported,[68,69] with increasing concentrations leading to drastic improvement in mechanical properties such as elastic modulus, strength, and rheological properties.[70–72]

Moreover, 20wt% RLP hydrogels exhibited the highest resilience amongst all concentrations almost certainly due to the significantly lower concentration of structural heterogeneities in comparison to the other concentrations, but also potentially due to formation of clusters of chains in the hydrogel (see below). We note that the magnitude of resilience for the RLP materials used in this study is considerably less than reported resilience values for previously published RLP hydrogels, likely due to the differences of sample preparation and mechanical characterization methods **(Figure S3).**[4]

To provide further insight into the change in network connectivity as a function of RLP polypeptide concentrations, the measured low-strain elastic moduli from microindentation (as well as from oscillatory shear rheology) were compared to the modulus predictions of the statistical theory of rubber elasticity. To calculate the theoretical elastic moduli using rubber elasticity, we first estimate the molecular weight between crosslinks, M_c in RLP hydrogels (listed in **Table 3**).[73] M_c values were determined from the crosslink density previously calculated for all RLP polypeptide concentrations (**Table 1**) by using the formula $M_c = \rho/N$, where ρ is the density of RLP and N is the total number of network strands per unit volume ($N=\nu_o f/2$).[74] The theoretical molecular weight between crosslinks thus decreases with an increase in crosslinking density due to the decrease in the length of the network strand between crosslink junctions, with M_c ranging from 279.9 ± 47.3 kg/mol for the 5wt% hydrogel, 131.6 ± 18.1 kg/mol in the 10wt% hydrogel, to 68.1 ± 8.7 kg/mol in the 20wt% hydrogel. For these calculations, the crosslinked network was assumed as an ideal network with Flory's assumptions: 1) all functional groups of the same type are equally reactive; 2) all groups react independently of one another; and 3) no intramolecular reactions occur in finite species.[75–77] Therefore, based on the calculation of M_c, the upper bound elastic modulus of the hydrogels can be estimated (E_{theory}) according to

$$E_{theory} = \frac{3\rho RT}{M_c}$$

where R is the gas constant and T is the temperature.[73] For the three RLP concentrations, we estimate E_{theory} to be 35.3 ± 5.5 kPa for 5wt%, 74.8 ± 11.0 kPa for 10wt% and 144.1 ± 17.3 kPa for 20wt% hydrogels (**Table 3**). These values are compared to the measured values of $E_{indentation}$ and $E_{rheology}$ in **Figure 6.**

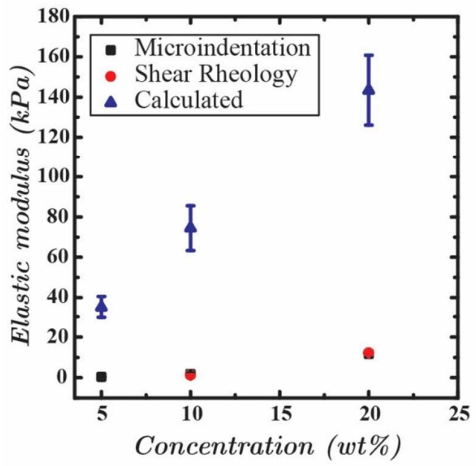

Figure 6 A comparison of elastic modulus measured from small-strain microindentation with elastic moduli obtained from oscillatory shear rheology at a comparable applied strain rate for RLP hydrogels. The microindentation and shear rheology data points nearly overlap, with both values significantly less than the calculated values.

Although good correlation of the moduli obtained from microindentation and oscillatory shear rheology is expected and confirms the linear elastic response of RLP hydrogels at small strains and millimeter length scales, the experimentally determined moduli are significantly lower than the moduli predicted by the statistical theory of rubber elasticity. Such differences in the predicted and measured elastic moduli almost certainly result from the fact that the RLP hydrogels are not perfectly crosslinked homogeneous networks, and structural defects such as an inhomogeneous distribution of crosslink junctions, dangling chain ends, and loops limit the appropriateness of statistical rubber elasticity theory for predicting the elastic moduli of these materials.[71,78,79]The reduced concentration of defects or elastically ineffective chains caused an increase in elastic moduli by ~12-fold upon doubling the RLP hydrogel concentration from 10wt% to 20wt%. On a further note, although we quantified the elastic modulus, $E_{indentation}$, for the 5wt% hydrogels assuming an elastic network, the resilience measurements do not indicate that a proper elastic network is formed at this concentration. Further, the permanent set observed for the 5wt% RLP hydrogels indicates that elastic analysis for moduli measurements is inappropriate for 5wt% hydrogels at least at strains larger than 10%.

To provide a semi-quantitative context for the impact of defects formed during RLP network formation process, we

employed the recently introduced real elastic network theory (RENT) to describe the effect of topological loops or cyclic defects on the bulk elasticity of polymer gels formed from A_2+B_3 and A_2+B_4 reactions.[39] Although the crosslinking reaction for the formation of RLP networks does not follow the A_2+B_3 stoichiometry, the average number of primary loops per crosslink junction n, which essentially act as dangling ends for a trifunctional crosslinker, can be approximated using the RENT theory. We do not consider the quantification of complex topological defects, such as secondary and tertiary loops, for this analysis since we do not have independent measurements of these species in the RLP hydrogels. Experimentally measured elastic moduli, $E_{indentation}$ for the three RLP concentrations (**from Figure 3(c)**) can be used to estimate the average number of primary loops per junction, n:

$$n = \frac{2}{5}\left(1 - \frac{E_{indentation}}{3NKT}\left(\frac{f}{f-2}\right)\right)$$

where N is the total number of network strands per unit volume ($N=\nu_o f/2$), f is the functionality of the cross-linker, and K is the Boltzmann constant, and T is the temperature. The calculated values of n are provided in **Table 3**.

Surprisingly, we found that n remained nearly identical for the 5wt% and 10wt% hydrogels, but decreased by ~27% in 20wt% hydrogels. These results suggest that while the number of crosslinking junctions correlates with the difference in elastic moduli for the 5wt% and 10wt% hydrogels, the significant decrease in the number of primary loops for the 20wt% hydrogels is likely responsible for the significant increase in their elastic modulus relative to that of the 10wt% hydrogels. From the resilience and small-strain microindentation results, it is clear that the proximity to c*, combined with the formation of loops at lower concentrations, contributes significantly to the network connectivity in the RLP hydrogels, as our data now demonstrate for these low concentration materials.

Table 3 Estimation of molecular weight between cross-links (M_c), elastic moduli (E_{theory}) from crosslink density of the RLP hydrogels, and fraction of primary loops as estimated by RENT theory.

c [a] (wt%)	Crosslinking density, ν_o (mol/L)	M_c (kg/mol)	E_{theory}(kPa)	Average number of primary loops, n
5	0.0032±0.0005	279.9±47.3	35.3±5.5	0.385±0.003
10	0.0068±0.0010	131.6±18.1	74.8±11.0	0.371±0.008
20	0.0131±0.0015	68.1±8.7	144.1±17.3	0.303±0.013

a Concentration of hydrogel

In addition, our studies permit, for the first time, quantification of the role of these network defects on large-strain response and failure properties. By comparing the results from the small-strain measurements to the large-strain indentation stiffness parameter, k'E, in **Table 4**, we observed strong correlation between small-strain elastic moduli and large-strain stiffness values across the three RLP polypeptide concentrations. Furthermore, this correlation suggests that the toe-shaped stress-strain relationships obtained from indentation experiments for these 5wt%, 10wt%, and 20wt% RLP hydrogels is self-consistent at larger deformations in that one elastic constant, e.g. the effective elastic modulus, can be used to capture the mechanical behavior of a given concentration hydrogel across a wide range of deformations. These results suggest that the nature of the network connectivity, or the nature of defects, is not significantly changing at larger strains. Similar stress-strain relationships have been previously measured from uniaxial tensile testing on 10wt% RLP gels.[29]

Table 4 Comparison of stiffness from small- strain microindentation, oscillatory shear rheology and puncture mechanics.

Concentration (wt%)	$E_{indentation}$ (kPa)	$E_{rheology}$ (kPa)	k'E(kPa)	E_{theory} (kPa)
5	0.45±0.06	Too soft to measure	0.10±0.02	35.3±5.5
10	1.83±0.61	1.32±0.06	2.08±0.20	74.8±11.0
20	11.65±1.25	12.18±0.70	15.82±2.8	144.1±17.3

Beyond indentation, the puncture experiments also provide the first insight into the effect of network connectivity and defects on the failure properties of RLP hydrogels. We have shown that the 20wt % RLP hydrogels show exceptionally high fracture initiation toughness, approximately 85 times more than the 5wt% hydrogels, and 10 times compared to the 10wt% hydrogels (**Figure 5(b)**). Although poor fracture resistance of the 5wt% hydrogels is not necessarily surprising given that they form a weak, underdeveloped network dominated by defects, the marked increase in failure initiation energy, Γ_o, for the 20wt% hydrogels compared to 10wt% hydrogels provides important insight into the structure-failure property relationship of RLP hydrogels formed at higher concentrations. In recent studies of solutions of Rec-1 resilin, it was found that at high polypeptide concentrations (above 10wt%), protein-protein intermolecular interactions dominate and result in molecular compaction and nanoscale aggregate formation.[63] We speculate that the nanoscale aggregates that arise from these RLP chain interactions may play an important role in increasing the resistance to crack nucleation in the 20wt% hydrogels and thus offer a tunable design parameter for these materials. In particular, the formation of nanoscale aggregates of appropriate size and distribution (rather than formation of a homogeneous network) may provide a network-level strategy for distributing the applied stress, increasing the total required energy for crack nucleation and localizing the crack nucleation to the inter-connected segments between the nanoscale aggregates. This distribution of stress, enabled by the distribution of nanoscale aggregates, may provide a mechanism for multiple cracks, or cavities, to be nucleated in close spatial and temporal proximity, thus leading to significant energy dissipation mechanisms. Similar mechanisms have been observed in nanoparticle-filled hydrogels, where weak interactions with distributed nanoparticles provide distributed sites for coordinated

delamination and associated dissipation.[80–82] Bimodal, or double network hydrogels, are also designed to provide enhanced fracture resistance by taking advantage of similar mechanisms.[83–85] Testing this hypothesized reinforcement mechanism in the higher concentration RLP hydrogels presents a significant experimental challenge, as neither the size nor the spatial distributions of the nanoscale aggregates are controlled in the current RLP hydrogels. Nevertheless, these results point to the importance of continued understanding of structure-property relationships in biopolymer hydrogels and their importance in the future design of robust pathways for soft materials with enhanced mechanical properties.

Conclusions

Structure-mechanical property relationships in RLP hydrogels of three different concentrations were investigated with three different mechanical characterization techniques at sub-millimeter and millimeter length scales. The RLP-based hydrogels were chosen as model materials for the study of mechanical properties, namely low-strain elasticity, resilience, large-strain deformation behavior and fracture initiation resistance, given their polarity and known propensity for inter-chain interactions. These chain properties permit correlation of mechanical properties with the evolution of inter-chain structure with increasing polypeptide concentration, an important feature of RLPs and other clinically and technologically important biomaterials. We found that RLP hydrogels possessed greatly improved elasticity and resilience at concentrations above the overlap concentration, c*, which favors homogeneous network formation with elastically effective inter-chain crosslinking and minimum structural heterogeneities. We also showed strong correlation between the low-strain elastic response measured via microindentation and oscillatory shear rheology; however, the ability to use existing network theories to reliably predict the elastic moduli was hampered by the development of network defects. Similarly, the minimization of network defects, especially at higher RLP concentrations, was suggested to correlate with increased resilience as a function of RLP polypeptide concentration even at higher applied strain. The ability of RLPs to form nanoscale aggregates in the 20wt% RLP hydrogels is speculated to play an important role in the development of their exceptionally high fracture initiation toughness. Overall, our results demonstrate and provide quantitative underpinning for the impact of underlying microstructure on the macroscopic properties of RLP hydrogels and highlight the ability to tailor their mechanical response, thus facilitating the design of soft yet resilient and tough biopolymer gels for future applications in regenerative medicine. Moreover, we have highlighted the ability of RLP hydrogels to exhibit non-linear elasticity, consistent with that observed for biological tissues and organs, while simultaneously maintaining excellent resilience and toughness, which further supports the use of RLPs as promising candidates for biomaterial tissue engineering.

Conflicts of interest

There are no conflicts to declare.

Acknowledgments

The authors acknowledge funding from the National Science Foundation (DMR 1609544), and the National Institute on Deafness and Other Communication Disorders (R01DC011377A), as well as instrument resources from the Delaware COBRE program, supported by grants from the National Institute of General Medical Sciences (1-P30-GM110758-01 and 1-P20-RR017716). We would also like to acknowledge Dr. Cesar Calero-Rubio for kind help with collection and analysis of scattering data.

Notes and references

1 T. Weis-Fogh, *J. Exp. Biol.*, 1960, **37**, 889–907.
2 H. Bennet-Clark, *J. Exp. Biol.*, 2007, **210**, 3879–3881.
3 N. Skals and A. Surlykke, *J. Exp. Biol.*, 1999, **202**, 2937–2949.
4 L. Li and K. L. Kiick, *ACS Macro Lett.*, 2013, **2**, 635–640.
5 L. Li, M. B. Charati and K. L. Kiick, *J. Polym. Sci. A. Polym. Chem.*, 2010, **1**, 1160–1170.
6 J. Gosline, M. Lillie, E. Carrington, P. Guerette, C. Ortlepp and K. Savage, *Philos. Trans. R. Soc. Lond. B. Biol. Sci.*, 2002, **357**, 121–32.
7 A. Girotti, D. Orbanic, A. Ibáñez-Fonseca, C. Gonzalez-Obeso and J. C. Rodríguez-Cabello, *Adv. Healthc. Mater.*, 2015, **4**, 2423–2455.
8 K. Bailey and T. Weis-Fogh, *Biochim. Biophys. Acta*, 1961, **48**, 452–459.
9 C. M. Elvin, A. G. Carr, M. G. Huson, J. M. Maxwell, R. D. Pearson, T. Vuocolo, N. E. Liyou, D. C. C. Wong, D. J. Merritt and N. E. Dixon, *Nature*, 2005, **437**, 999–1002.
10 S. Lv, D. M. Dudek, Y. Cao, M. M. Balamurali, J. Gosline and H. Li, *Nature*, 2010, **465**, 69–73.
11 C. L. McGann, E. A. Levenson and K. L. Kiick, *Macromolecules*, 2013, **214**, 203–213.
12 Y. Kim, E. E. Gill and J. C. Liu, *Biomacromolecules*, 2016, **17**, 2530–2539.
13 L. Li, A. Mahara, Z. Tong, E. A. Levenson, C. L. McGann, X. Jia, T. Yamaoka and K. L. Kiick, *Adv. Healthc. Mater.*, 2016, **5**, 266–75.
14 R. E. Lyons, E. Lesieur, M. Kim, D. C. C. Wong, M. G. Huson, K. M. Nairn, A. G. Brownlee, R. D. Pearson and C. M. Elvin, *Protein Eng. Des. Sel.*, 2007, **20**, 25–32.
15 M. Kim, C. Elvin, A. Brownlee and R. Lyons, *Protein Expr. Purif.*, 2007, **52**, 230–236.
16 K. M. Nairn, R. E. Lyons, R. J. Mulder, S. T. Mudie, D. J. Cookson, E. Lesieur, M. Kim, D. Lau, F. H. Scholes and C. M. Elvin, *Biophys. J.*, 2008, **95**, 3358–3365.
17 N. K. Dutta, M. Y. Truong, S. Mayavan, N. R. Choudhury, C. M. Elvin, M. Kim, R. Knott, K. M. Nairn and A. J. Hill, *Angew. Chemie Int. Ed.*, 2011, **50**, 4428–31.
18 L. Li, T. Luo and K. L. Kiick, *Macromol. Rapid Commun.*,

2015, **36**, 90–95.
19 A. M. Tamburro, S. Panariello, V. Santopietro, A. Bracalello, B. Bochicchio and A. Pepe, *ChemBioChem*, 2010, **11**, 83–93.
20 A. Bracalello, V. Santopietro, M. Vassalli, G. Marletta, R. Del Gaudio, B. Bochicchio and A. Pepe, *Biomacromolecules*, 2011, **12**, 2957–65.
21 C. L. McGann, R. E. Akins and K. L. Kiick, *Biomacromolecules*, 2016, **17**, 128–140.
22 H. K. Lau, L. Li, A. K. Jurusik, C. R. Sabanayagam and K. L. Kiick, *ACS Biomater. Sci. Eng.*, 2017, **3**, 757–766.
23 J. L. Whittaker, N. K. Dutta, R. Knott, G. McPhee, N. H. Voelcker, C. Elvin, A. Hill and N. R. Choudhury, *Langmuir*, 2015, **31**, 8882–8891.
24 S. Lv, T. Bu, J. Kayser, A. Bausch and H. Li, *Acta Biomater.*, 2013, **9**, 6481–6491.
25 L. Li, Z. Tong, X. Jia and K. L. Kiick, *Soft Matter*, 2013, **9**, 665–673.
26 Y. Kim, J. N. Renner and J. C. Liu, *Biomater. Sci.*, 2014, **2**, 1110–1119.
27 Y. Kim and J. C. Liu, *Biomater. Sci.*, 2016, **4**, 1761–1772.
28 M. B. Charati, J. L. Ifkovits, J. A. Burdick, J. G. Linhardt and K. L. Kiick, *Soft Matter*, 2009, **5**, 3412–3416.
29 L. Li and K. Kiick, *Front. Chem.*, 2014, **2**, 20–32.
30 L. Li, S. Teller, R. J. Clifton, X. Jia and K. L. Kiick, , DOI:10.1021/bm200373p.
31 R. Liu and W. Oppermann, *Macromolecules*, 2006, **39**, 4159–4167.
32 S. Seiffert, *Prog. Polym. Sci.*, 2017, **66**, 1–21.
33 E. M. Saffer, M. A. Lackey, D. M. Griffin, S. Kishore, G. N. Tew and S. R. Bhatia, *Soft Matter*, 2014, **10**, 1905–16.
34 F. Di Lorenzo and S. Seiffert, *Polym. Chem.*, 2015, **6**, 5515–5528.
35 S. Seiffert, *Polym. Chem.*, 2017, **3**, 4472–4487.
36 P. J. Flory, *Polymer (Guildf).*, 1985, 17, 1–12.
37 Y. Akagi, T. Katashima, Y. Katsumoto, K. Fujii, T. Matsunaga, U.-I. Chung, M. Shibayama and T. Sakai, *Macromolecules*, 2011, **44**, 5817–5821.
38 Y. Akagi, J. P. Gong, U. Chung and T. Sakai, *Macromolecules*, 2013, **46**, 1035–1040.
39 M. Zhong, R. Wang, K. Kawamoto, B. D. Olsen and J. A. Johnson, *Science (80-.).*, 2016, **353**, 1264–1268.
40 P. de Gennes, 1979.
41 K. Nishi, H. Asai, K. Fujii, Y.-S. Han, T.-H. Kim, T. Sakai and M. Shibayama, *Macromolecules*, 2014, **47**, 1801–1809.
42 K. R. Shull, *Contact mechanics and the adhesion of soft solids*, 2002, vol. 36.
43 S. Fakhouri, S. B. Hutchens and A. J. Crosby, *Soft Matter*, 2015, **11**, 4723–4730.
44 W. G. Herrick, S. Rattan, T. V Nguyen, M. S. Grunwald, C. W. Barney, A. J. Crosby and S. R. Peyton, *Cell. Mol. Bioeng.*, 2015, **8**, 333–348.
45 L. E. Jansen, N. P. Birch, J. D. Schiffman, A. J. Crosby and S. R. Peyton, *J. Mech. Behav. Biomed. Mater.*, 2015, **50**, 299–307.
46 H. Luyten and T. Van Vliet, *J. Texture Stud.*, 1995, **26**, 281–298.
47 A. Ghatak, K. Vorvolakos, H. She, D. L. Malotky and M. K. Chaudhury, *J. Phys. Chem. B*, 2000, **104**, 4018–4030.
48 M. E. Seitz, D. Martina, T. Baumberger, V. R. Krishnan, C.-Y. Hui and K. R. Shull, *Soft Matter*, 2009, **5**, 447–456.
49 M. J. Buehler and S. Keten, *Nano Res.*, 2008, **1**, 63.
50 J. Cui, M. A. Lackey, G. N. Tew and A. J. Crosby, *Macromolecules*, 2012, **45**, 6104–6110.
51 K. R. Shull, D. Ahn, W.-L. Chen, C. M. Flanigan and A. J. Crosby, *Macromol. Chem. Phys.*, 1998, **199**, 489–511.
52 *Biomaterials*, 1996, **17**, 1647–1657.
53 A. C. Fischer-Cripps, *Introduction to Contact Mechanics*, Springer Science, Second., 2007.
54 G. A. Holzapfel, *Handb. Mater. Behav. Model.*, 2001, **3**, 1049–1063.
55 B. Xu, Y. Li, X. Fang, G. A. Thouas, W. D. Cook, D. F. Newgreen and Q. Chen, *J. Mech. Behav. Biomed. Mater.*, 2013, **28**, 354–365.
56 J. Gary Lin and C.H. Newton., *ANTEC 87 ,Conference Proceedings. Soc. Plast. Eng.*
57 M. Carfagni, E. Lenzi and M. Pierini, *Proceedings-spie Int. Soc. Opt. Eng.*, 1998, **1**, 580–584.
58 T. Trakulsujaritchok and D. J. Hourston, *Eur. Polym. J.*, 2006, **42**, 2968–2976.
59 K. R. Rajagopal and A. S. Wineman, *Int. J. Plast.*, 1992, **8**, 385–395.
60 M. Mihajlovic, M. Staropoli, M.-S. Appavou, H. M. Wyss, W. Pyckhout-Hintzen and R. P. Sijbesma, *Macromolecules*, 2017, **50**, 3333–3346.
61 W. W. Graessley, *Polymer (Guildf).*, 1980, **21**, 258–262.
62 Q. Ying and B. Chu, *Macromolecules*, 1987, **20**, 362–366.
63 R. Balu, J. P. Mata, R. Knott, C. M. Elvin, A. J. Hill, N. R. Choudhury and N. K. Dutta, *J. Phys. Chem. B*, 2016, **120**, 6490–6503.
64 A. H. Clark and S. B. Ross-Murphy, *Br. Polym. J.*, 1985, **17**, 164–168.
65 S. Kasapis, *Int. J. Food Sci. Technol.*, 1994, **29**, 29–38.
66 R. Kappiyoor, G. Balasubramanian, D. M. Dudek and I. K. Puri, *Soft Matter*, 2011, **7**, 11006–11009.
67 H. H. Winter and F. Chambon, *J. Rheol. Imbalanced Stoichiom. J. Rheol. J. Chem. Phys. Rubberlike Elast. J. Chem. Phys. Viscoelasticity J. Rheol. J. Rheol.*, 1986, **301**, 1272–201.
68 C. Michon, G. Cuvelier and B. Launay, *Rheol. Acta Rheol Acta*, 1993, **32**, 94–103.
69 S. Panyukov and Y. Rabin, *Phys. Rep.*, 1996, **269**, 1–131.
70 T. Sakai, T. Matsunaga, Y. Yamamoto, C. Ito, R. Yoshida, S. Suzuki, N. Sasaki, M. Shibayama and U. Il Chung, *Macromolecules*, 2008, **41**, 5379–5384.
71 P. Malo de Molina, S. Lad, M. E. Helgeson, P. M. De Molina, S. Lad and M. E. Helgeson, *Macromolecules*, 2015, **48**, 5402–5411.
72 Y. Gu, K. Kawamoto, M. Zhong, M. Chen, M. J. A. Hore, A. M. Jordan, L. T. J. Korley, B. D. Olsen and J. A. Johnson, *Proc. Natl. Acad. Sci.*, 2017, **114**, 4875–4880.
73 G. Treloar and L. R. G. Treloar, *Rep. Prog. Phys. Rep. Prog. Phys*, 1973, **36**, 755–755.
74 M. Rubinstein and R. H. Colby, *Polymer Physics*, Oxford University Press, New York, 2003.

75 P. J. Flory, *J. Am. Chem. Soc.*, 1941, **63**, 3083–3090.
76 C. W. Macosko and D. R. Miller, *Macromolecules*, 1976, **9**, 199–206.
77 L. W. Hill, *Prog. Org. Coatings*, 1997, **31**, 235–243.
78 F. Di Lorenzo, J. Hellwig, R. von Klitzing and S. Seiffert, *ACS Macro Lett.*, 2015, **4**, 698–703.
79 W. Chassé, M. Lang, J.-U. Sommer and K. Saalwächter, *Macromolecules*, 2012, **451. Chass**, 899–912.
80 K. Haraguchi and T. Takehisa, *Adv. Mater.*, 2002, **14**, 1120–1124.
81 Y. Shona Pek, A. C. A. Wan, A. Shekaran, L. Zhuo and J. Y. Ying, *Nat. Nanotechnol.*, 2008, **3**, 671–675.
82 A. K. Gaharwar, N. a Peppas and A. Khademhosseini, *Biotechnol. Bioeng.*, 2014, **111**, 441–453.
83 J. P. Gong, Y. Katsuyama, T. Kurokawa and Y. Osada, *Adv. Mater.*, 2003, **15**, 1155–1158.
84 J.-Y. Sun, X. Zhao, W. R. K. Illeperuma, O. Chaudhuri, K. H. Oh, D. J. Mooney, J. J. Vlassak and Z. Suo, *Nature*, 2012, **489**, 133–6.
85 E. Ducrot, Y. Chen, M. Bulters, R. P. Sijbesma and C. Creton, *Science (80-.).*, 2014, **344**, 186–189.

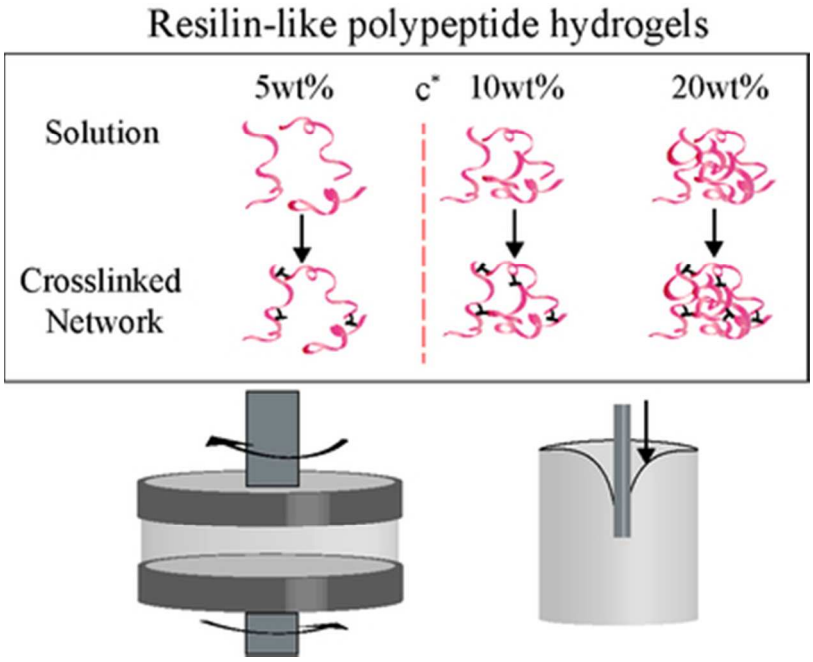

34x27mm (300 x 300 DPI)